Photoreconstructions

DOI: 10.1002/anie.201402515

Following a Photoinduced Reconstructive Phase Transformation and its Influence on the Crystal Integrity: Powder Diffraction and Theoretical Study**

Tomče Runčevski, Marina Blanco-Lomas, Marco Marazzi, Marcos Cejuela, Diego Sampedro,* and Robert E. Dinnebier*

Abstract: *In the course of solid-state photoreactions, a single crystal (SC) of the reactant can be transformed into an SC of the product or it can lose crystallinity and become amorphous. In-between these two scenarios exist the reconstructive phase transformations, where upon irradiation, the reactant SC becomes a powder or an SC with increased mosaicity. We present a detailed description of reconstructive photodimerization, where the structural changes are directly correlated with the disintegration process. The kinetics of the reaction is explained by two kinetic regimes, forming an autocatalytic autoinhibition photoreaction set with high quantum yield. In addition, the photoreaction pathways were studied theoretically.*

The first report on photoinduced reactions of organic crystals dates back to the 19th century; the topochemical principle was postulated based on the intensive research on solid-state photoreactions that followed.[1] This very intuitive and exceedingly useful concept employs the necessity of minimum geometrical changes in constrained environments such as the crystal packing. Topotactic reactions are those in which the product forms in an oriented fashion, requiring at least some lattice points to coincide with the lattice points of the reactant.[2] Most of these reactions are reversible and proceed in a single-crystal-to-single-crystal (SCSC) manner, which represents a promising platform for the design of photoswitches and molecular motors.[3] There are examples, however, of irreversible photoamorphization and/or melting reactions.[4] In between these two reaction types exist the so-called reconstructive phase transformations (RPTs).[4b] When the geometrical movements during the reaction are significant (in the sense of different crystal packings, accommodated in different unit cells), the crystal cannot withstand the stress and therefore disintegrates.[5] The crystal disintegration and irreversibility of the reaction hamper the perspective applications of RPT systems in molecular machineries. Contrary, in terms of synthetic photochemistry, irreversible high-yield RPT reactions are very favorable. Thus, tuning the reaction fashion stands at the frontiers of modern crystal engineering. The borders between the realms of SCSC and RPT reactions are not impassable, for instance dilution of the crystal packing with single water molecules can change the type of the reaction from RPT to SCSC.[5b,c]

In order to better understand RPTs, knowledge on the structure before and after the photoreaction is crucial. Generally, small organic molecules build SCs suitable for single-crystal X-ray diffraction (SCXRD). In RPTs, however, the crystal disintegrates upon irradiation, thwarting the structure solution of the products. For example, it was recently reported that crystals of molecules resembling the green fluorescent protein (GFP) chromophore, disintegrate when they dimerize under exposure to UV light.[5a] Recrystallization of stable photoproducts, followed by ex situ analysis is not always applicable, as it often leads to different polymorphs. There are reported strategies for favoring SCSC reactions and enabling the solution of the crystal structures of the photoproducts (for example using reduced flux of irradiation, sometimes at low temperature). Those photoproducts generally have a different crystal structure compared to the photoproducts obtained by RPT. The former products are obtained through a topotactic reaction and have similar unit cells as the reactant, while the latter have significantly different unit cells (and that difference effectively causes the crystal disintegration). In general, disintegration of a crystal means reduction to sizes not suitable for the current SC diffractometers and/or a substantial increase of the mosaicity. These serious problems for SCXRD can be overcome by using X-ray powder diffraction (XRPD). Beside the advances in instrumentation and software, crystal-struc-

[*] T. Runčevski, Prof. R. E. Dinnebier
Max-Planck-Institute for Solid State Research
Heisenbergstrasse 1, 70569 Stuttgart (Germany)
E-mail: t.runcevski@fkf.mpg.de
Dr. M. Blanco-Lomas, M. Cejuela, Dr. D. Sampedro
Departamento de Química, Universidad de La Rioja
Madre de Dios, 54, 26006 La Rioja (Spain)
E-mail: diego.sampedro@unirioja.es
Dr. M. Marazzi
Department of Theoretical Chemical Biology
Institute of Physical Chemistry, KIT
Kaiserstrasse 12, 76131 Karlsruhe (Germany)
and
Departamento de Química Analítica, Química Física e Ingeniería Química, Universidad de Alcalá
28871 Alcalá de Henares (Spain)

[**] D.S. acknowledges the Spanish Ministerio de Ciencia e Innovación (MICINN)/Fondos Europeos para el Desarrollo Regional (FEDER) (CTQ2011-24800). M.B.-L. thanks the Spanish Ministerio de Educación y Ciencia (MEC) for a grant. M.M. acknowledges the UAH (Universidad de Alcalá) and the Alexander von Humboldt Foundation. T.R. thanks the IMPRS-CMS. Andrea Knöller is acknowledged for recording the SEM images and Frank Adams for designing the photochamber.

Supporting information for this article is available on the WWW under http://dx.doi.org/10.1002/anie.201402515.

ture solution by XRPD appears to be a niche technique. It should be noted that while the deviation of precise intramolecular parameters by XRPD is hampered by its intrinsic technical problems,[6] intermolecular features are certainly much better defined, as they depend on collective properties of the molecular models, and on the lattice symmetry and periodicity, which in fact are more relevant to the study of RPT. Moreover, XRPD, unlike SCXRD, provides information on the average structure of the bulk, and provides additional information, such as domain size, the presence of defects, faults, and strain, among other.[6]

Benzylidene oxazolones are photoactive compounds that, surprisingly, have been scarcely explored in terms of photoreactivity.[7] A member of this family is the (*Z*)-4-(4-bromobenzylidene)-2-methyloxazol-5(4*H*)-one system (*Z*-**1**). As evident from the UV spectrum (Figure S1 in the Supporting Information), a range of wavelengths can be used to promote its photoreactivity. When irradiated in solution under a variety of conditions, *Z*–*E* photoisomerization was the main photoreaction (Scheme 1 a). However, when placed on a plate and

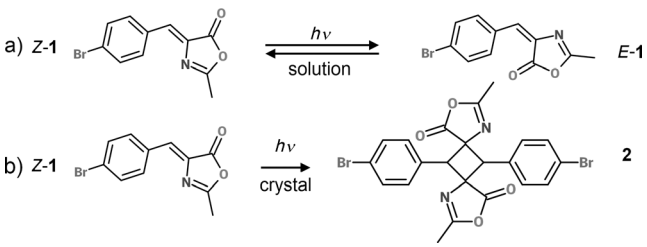

Scheme 1. a) Solution photoisomerization and b) solid-state photodimerization.

irradiated at 350 nm using a photoreactor, no isomerization was detected by ^{1}H NMR spectroscopy. Instead, dimer **2**, a product of a [2+2] photocycloaddition, was observed (Scheme 1 b). After five days of irradiation, **2** was found in the reaction crude in a 90 % yield. The resulting crude was purified by chromatography on silica gel and the product was confirmed to be **2** by ^{1}H and ^{13}C NMR spectroscopy and HRMS (Figures S2 and S3 in the Supporting Information). To check the stability of **2**, several trials were conducted with samples that were obtained directly from the reaction crude after irradiation, and no decomposition of **2** was found (see the Supporting Information).

Crystals of *Z*-**1** were monitored on the course of the irreversible photoreaction with scanning transmission microscopy (SEM) and XRPD. Figure 1 shows the irreversible crystal disintegration as the reaction proceeds, followed by changes of the diffraction patterns. Accordingly, the photoreaction outlined in Scheme 1 b turns out to be a perfect model for studying of RPT reaction by correlating the macroscopic effects on the crystals with molecular movements in the structure during the reaction.

Attempts to grow crystals of *Z*-**1** suitable for SCXRD resulted in microcrystalline powders. The in situ synthesis of **2** led to an even more "powdered" sample. Therefore, the crystal structures were determined using high-resolution laboratory XRPD. Indexing was performed from first princi-

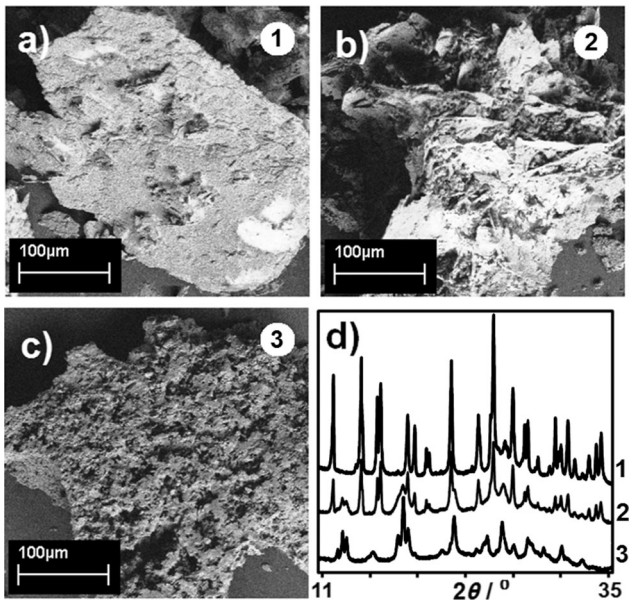

Figure 1. SEM images of crystals of *Z*-**1** a) before irradiation, and after b) 3 days and c) 5 days of irradiation. d) Respective XRPD patterns.

ples through the iterative use of singular value decomposition, followed by a Pawley fitting and a simulating annealing approach to solve the crystal structures. The structure models were refined by the Rietveld method (for details see the Supporting Information). *Z*-**1** crystallizes in an orthorhombic unit cell (space group $Pbc2_1$) with two molecules in the asymmetric unit (denoted **A** and **B**). The main difference between the symmetrically independent molecules is the torsion angle between both rings (N-C4-C5-C6 in **A** = 3.84° and in **B** = −16.67°, see CIF in Supporting Information). The two molecules are closely head-to-tail packed, where the distances between the double bond carbon atoms are C**A**4–C**B**5 = 3.375 Å and C**A**5–C**A**4 = 3.625 Å, making the pairs aligned parallel to the *a*-axis (Figure 2 a). The Hirshfeld surfaces around the C4 and C5 atoms of both molecules show intensive contacts, which together with the C−C distances smaller than 4.2 Å (the Schmidt criterion for photocycloaddition)[1] explain the photoreactivity of *Z*-**1** and formation of dimer **2.** The dimer crystallizes in the low symmetry, triclinic $P\bar{1}$ space group with half a molecule (one respective monomer) in the asymmetric unit. Figure 2 b shows the necessary molecular movements of the **A** and **B** monomers in order to form the dimer molecule. The five-membered rings perform remarkable bending, whereas the heavier six-membered ring is slightly rotated.

In order to accommodate the new geometry of the dimer product, the crystal packing significantly changes. In the reactant, the monomers are packed forming two layers (depicted in green and blue, Figure 2 d), whereas the dimers in the product become ordered in one layer (Figure 2 e). For this transformation to happen, significant molecular movements (such as in-layer rotation and shifting) must occur. Those movements generate immense internal stress which, when released, triggers disintegration of the crystal. The result of this disintegration is visible in Figure 1. We

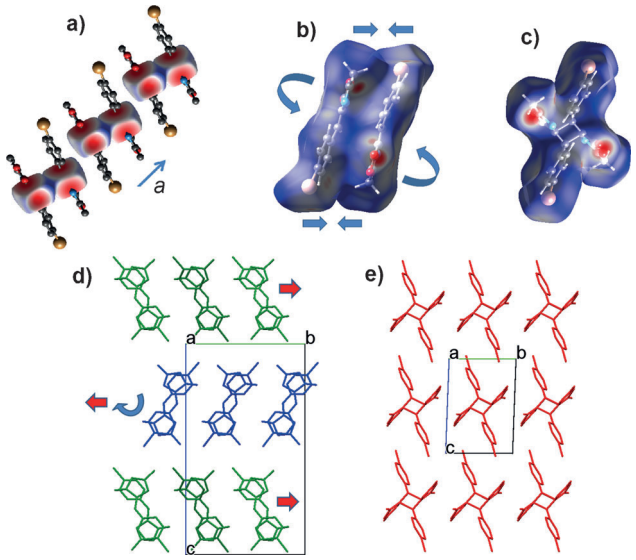

Figure 2. a) Head-to-tail packed monomers along the *a*-axis and the Hirshfeld surface around the reactive bonds. Hirshfeld surfaces of b) the monomers in *Z*-**1**, and c) the dimer in **2**. Crystal packing diagrams of d) *Z*-**1** and e) **2**.

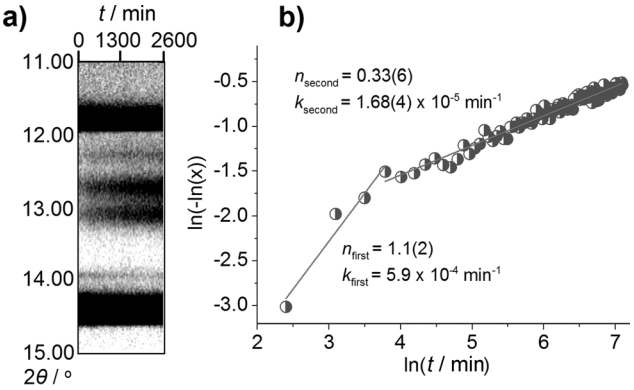

Figure 3. a) 2D projection of the observed X-ray intensity as a function of diffraction angle and time. c) Sharp–Hancock plot of the reaction.

calculated the domain size as the reaction proceeds and found that the domain size of the product particles reduces by approximately 50% compared to the domain size of the reactant (see the Supporting Information).

To explain the nature of the photoreaction and crystal disintegration, information on the nucleation and the subsequent growth of the product phase is needed. There are many cases where the kinetics of such reactions is explained using the JMAK model.[8] The model is centered around the equation $\ln(-\ln(1-x)) = n\ln(t) + n\ln(k)$. The Sharp–Hancock plot is representable for such a model and gives a straight line with a slope n and intercept $n\ln(k)$, where t is the time to collapse, $x(t)$ is the evolved fraction of the product phase, k (s^{-1}) is the reaction rate constant, and n is the Avrami exponent. The rate constant k depends on the nucleation and growth rates and is also sensitive to temperature. The Avrami exponent represents the order of the reaction and describes the dimensionality of the growth of the product phase. It relates to the dimensionality (dim) of the growth of the dimer with the equation $\dim = n-1$. Interestingly, the Sharp–Hancock plot of the collected data of the *Z*-**1** dimerization exhibits two different growth regimes (Figure 3).

The first regime explains the kinetic behavior at the beginning of the reaction. Inspecting the slope and intercept of the plot gives $k_{first} = 5.9(5)\times10^{-4}\,min^{-1}$ and $n_{first} = 1.1(2)$. These values indicate a fast reaction in connection with homogeneous nucleation.[8] We believe that during this regime, photocycloaddition takes place in an SCSC manner. With minimal molecular movements, the monomers dimerize. Upon further irradiation, the product is formed and accommodated in the unit cell of the reactant, thus forming a solid-solution mixture. The molecular geometries of the reactant and the product (Figure 2b and c) significantly differ. Accordingly, soon after its formation, the product molecules collectively move, accommodating in a thermodynamically more favorable crystal packing. This reconstruction transition is assumed to happen during the second regime in the kinetics plot; $k_{second} = 1.68(4)\times10^{-5}\,min^{-1}$ and $n_{second} = 0.33(6)$. The dimensionality of the process has a negative value, which can be described by including a negative autocatalytic step, termed autoinhibition.[10] We assume that the disintegration of the crystal acts as an inhibition step to the photoreaction by cracking and reducing the domains, thus influencing the nucleation rate and growth of the dimer phase in the reacting matrix of the monomer phase. However, the fragmentation of the particles enables easier penetration of photons inside the reacting crystal, making the bulk material accessible to irradiation. Thus, it can be suggested that the fragmentation leads to a fine balance between kinetics inhibition and fragmentation-assisted bulk phototransformation. The interplay between the homogenously reacting first regime and fragmentation-effect-dominated second regime leads to unique photoreaction set with (theoretically) 100% yield.

In order to gain insights into the processes before the SCSC and RPT reactions, a series of theoretical calculations on the photoreaction were performed (Figure 4). The experimental absorption spectrum of *Z*-**1** in the solid state was used to validate the model by time-dependent density functional theory (TD-DFT) at the CAM-B3LYP/6-31+G* level.[9] Calculations were performed on the whole unit cell with the Gaussian 09 program package (see the Supporting Information for the reference). For the $S_0 \rightarrow S_1$ and $S_0 \rightarrow S_2$ transitions, more than one electronic configuration is involved per electronic state (Table S2 in in the Supporting Information). In the case of the optically bright S_2 state, most of the configurations describe an excitation localized on four head-to-tail facing molecules, that is, two dimers, with some contributions from single-monomer excitations (Figure S7 in the Supporting Information).

This delocalization over the unit cell is in agreement with the experimental results, considering that **2** is promoted by a dimer initially arranged in a head-to-tail conformation. In order to reliably take into account the multiconfigurational nature of the observed electronic excitations, the MS-CASPT2//SA-CASSCF methodology[10] was applied with an affordable ANO-S basis set to one of the solved dimer structures. The computed absorption spectrum using the MOLCAS 7.6 package[11] (see the Supporting Information) is

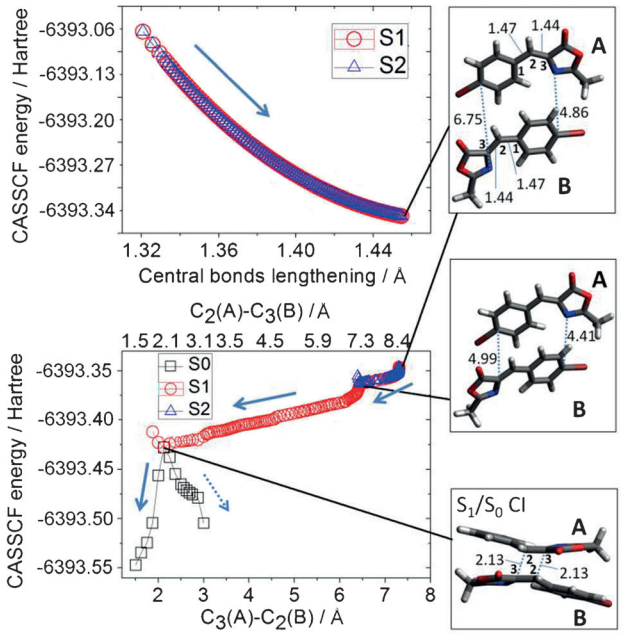

Figure 4. Excited-state pathways as a function of the most relevant coordinates. Top: Initial relaxation on S_2 and S_1 states. The central-bonds-lengthening coordinate is defined as the average of C1–C2 and C2–C3 bond lengths of both molecules, **A** and **B**. Bottom: Continuation of the pathway, as a function of the two C2–C3 intermolecular distances, including S_2/S_1 energy degenerate region and S_1/S_0 conical intersection (CI), which funnels the formation of the photoproduct on the ground state (blue arrows), the less favored route is represented by a dashed blue line.

in accordance with the one calculated at the TD-DFT level for the whole unit cell. The selected active space comprises, for each of the two molecules, one set of π and π* orbitals centered on the C2–C3 formal double bond (Figure 4), one set of π and π* orbitals centered on the Ph-Br moiety, and one set of π and π* orbitals delocalized over the chromophore, overall including 12 electrons in 12 orbitals. At this level of theory, the dimer absorption properties qualitatively match with TD-DFT results, therefore allowing us to study the formation of the photoproduct through multiconfigurational quantum chemistry (Table S3 in the Supporting Information). After absorption at the Franck–Condon region, minimum-energy paths were calculated from S_2 (Figure 4). The overall mechanism can be separated into two parts. The first step consists of bond lengthening of the **A** and **B** molecules, with almost identical energy relaxation in S_2 and S_1 states, both $^1(\pi,\pi^*)$ states (Figure 4, top). This first step increases the structural flexibility. Then, the orbital overlapping resulting from π–π stacking generates attraction between **A** and **B** molecules. This therefore allows breaking the degeneracy in energy between S_2 and S_1, further dissipating the excitation energy in S_1 up to a conical intersection with the ground state (S_1/S_0 CI), where the dimer has an almost symmetrical geometry, with **A** facing **B** and an equivalent intermolecular distance between C2 and C3 atoms of 2.13 Å (Figure 4, bottom). This type of CI is similar to those found for photochemical pericyclic reactions.[12] From the S_1/S_0 CI, two pathways are available: formation of **2** or recovery of the initial structure (i.e. internal conversion). Considering the steepness of the S_0, and especially the high vibrational excess calculated from the Franck–Condon region, the photochemical pathway should preferentially lead to the formation of **2**, thus expecting high quantum yield (i.e. no side reactions, no fluorescence and almost no internal conversion). This mechanism is in agreement with the experimental findings and suggests that a theoretical yield of 100% is possible.

To summarize, the photoreaction proceeds through a minimum of three consecutive steps upon photoirradiation. The first one is photoexcitation. The physics of this process, with the accent on the excited-state pathways, is explained by using quantum mechanical calculations. During the second one, photodimerization of the monomer molecules takes place, assuming an SCSC reaction manner. During the last process, a collective molecular movement happens, causing an RPT, which results in irreversible disintegration of the crystals. For the first time, the latter, important macroscopic event is correlated with the significant changes on molecular level in the crystal structures before and after the photoreaction. These (in situ followed) changes of the crystal packing (in-layer rotations and molecules shifting) create immense internal stress, which when released causes the disintegration of the crystals. The kinetics of this photodimerization reaction supports the postulated reaction model and is explained by two different kinetic regimes upon photoexcitation, the second one representing an interesting autocatalytic auto-inhibition RPT photoreaction set, disintegrating the crystal and giving dimer products with high quantum yields (the experimental quantum yield after five days of irradiation reached 90%).

Received: February 17, 2014
Published online: May 21, 2014

Keywords: excited states · oxazolones · phase transformations · photodimerization · powder diffraction

[1] a) S. Trommsdorff, *Ann. Chem. Pharm.* **1834**, 11; b) H. I. Bernstein, W. C. Quimby, *J. Am. Chem. Soc.* **1943**, *65*, 1845; c) M. D. Cohen, G. M. J. Schmidt, *J. Chem. Soc.* **1964**, 1996.

[2] H. Morawetz, S. Z. Jakabhazy, J. B. Lando, J. Shafer, *Proc. Natl. Acad. Sci. USA* **1963**, *49*, 789–793.

[3] a) S.-Y. Yang, P. Naumov, S. Fukuzumi, *J. Am. Chem. Soc.* **2009**, *131*, 7247; b) K. Tanaka, F. Toda, E. Mochizuki, N. Yasui, Y. Kai, I. Miyahara, K. Hirotsu, *Angew. Chem.* **1999**, *111*, 3733; *Angew. Chem. Int. Ed.* **1999**, *38*, 3523; c) N. L. Toh, M. Nagarathinam, J. J. Vittal, *Angew. Chem.* **2005**, *117*, 2277; *Angew. Chem. Int. Ed.* **2005**, *44*, 2237; d) M. H. Mir, L. L. Koh, G. K. Tan, J. J. Vittal, *Angew. Chem.* **2010**, *122*, 400; *Angew. Chem. Int. Ed.* **2010**, *49*, 390; e) S. D. Karlen, H. Reyes, R. E. Taylor, S. I. Khan, M. F. Hawthorne, M. A. Garcia-Garibay, *Proc. Natl. Acad. Sci. USA* **2010**, *107*, 14973; f) M. Nagarathinam, A. M. P. Peedikakkal, J. J. Vittal, *Chem. Commun.* **2008**, 5277; g) S.-Y. Yang, X.-L. Deng, R.-F. Jin, P. Naumov, M. K. Panda, R.-B. Huang, L.-S. Zheng, B. K. Teo, *J. Am. Chem. Soc.* **2014**, *136*, 558; h) V. Enkelmann, G. Wegner, K. Novak, K. B. Wagener, *J. Am. Chem. Soc.* **1993**, *115*, 10390.

[4] a) P. Naumov, P. Makreski, G. Petruševski, T. Runčevski, G. Jovanovski, *J. Am. Chem. Soc.* **2010**, *132*, 14973; b) D. de Loera,

A. Stopin, M. A. Garcia-Garibay, *J. Am. Chem. Soc.* **2013**, *135*, 6626.

[5] a) P. Naumov, J. Kowalik, K. M. Solntsev, A. Baldridge, J.-S. Moon, C. Kranz, L. M. Tolbert, *J. Am. Chem. Soc.* **2010**, *132*, 5845; b) N. K. Nath, K. Manoj, A. S. Gac, P. Naumov, *Chem. Eur. J.* **2013**, *19*, 8094; c) Water molecules also influence the crystallinity during the crystallization processes, T. Runčevski, G. Petruševski, P. Makreski, S. Ugarkovic, R. E. Dinnebier, *Chem. Commun.* **2014**, DOI: 10.1039/c4cc01430h.

[6] R. E. Dinnebier, S. J. L. Billinge, *Powder Diffraction: Theory and Practice*, RSC Publishing, Cambridge, **2008**.

[7] a) M. Blanco-Lomas, P. J. Campos, D. Sampedro, *Org. Lett.* **2012**, *14*, 4334; b) I. Funes-Ardoiz, M. Blanco-Lomas, P. J. Campos, D. Sampedro, *Tetrahedron* **2013**, *69*, 9766.

[8] a) M. Avrami, *J. Chem. Phys.* **1939**, *7*, 1103; b) W. A. Johnson, P. A. Mehl, *Trans. AIME* **1939**, *135*, 416; c) A. N. Kolmogorov, *Bull. Acad. Sci. USSR Phys. Ser.* **1937**, *1*, 355; d) R. Medishetty, A. Husain, Z. Bai, T. Runčevski, R. E. Dinnebier, P. Naumov, J. J. Vittal, *Angew. Chem.* **2014**, DOI: 10.1002/ange.201402040; *Angew. Chem. Int. Ed.* **2014**, DOI: 10.1002/anie.201402040; e) A. F. Mabied, M. Mueller, R. E. Dinnebier, S. Nozawa, M. Hoshino, A. Tomita, T. Sato, S. Adachi, *Acta Crystallogr. Sect. B* **2012**, *68*, 424; f) R. Moré, G. Busse, J. Hallmann, C. Paulmann, M. Scholz, S. Techert, *J. Phys. Chem. C* **2010**, *114*, 4142; g) J. B. Benedict, P. Coppens, *J. Phys. Chem. A* **2009**, *113*, 3116.

[9] a) T. Yanai, D. P. Tew, N. C. Handy, *Chem. Phys. Lett.* **2004**, *393*, 51; b) V. Voliani, R. Bizzarri, R. Nifosì, S. Abbruzzetti, E. Grandi, C. Viappiani, F. Beltram, *J. Phys. Chem. B* **2008**, *112*, 10714.

[10] K. Andersson, P.-Å. Malmqvist, B. O. Roos, A. J. Sadlej, K. Wolinski, *J. Phys. Chem.* **1990**, *94*, 5483 – 5488.

[11] F. Aquilante, L. De Vico, N. Ferré, G. Ghigo, P.-Å. Malmqvist, P. Neogrády, T. B. Pedersen, M. Pitonak, M. Reiher, B. O. Roos, L. Serrano-Andrés, M. Urban, V. Veryazov, R. Lindh, *J. Comput. Chem.* **2010**, *31*, 224 – 247.

[12] F. Bernardi, M. Olivucci, M. A. Robb, *J. Photochem. Photobiol. A* **1997**, *105*, 365.

